UC Irvine
UC Irvine Previously Published Works

Title
Analysis and visualization method for understanding the voltage effect of distributed energy resources on the electric power system

Permalink
https://escholarship.org/uc/item/4h4496fm

Journal
Electric Power Systems Research, 82(1)

ISSN
0378-7796

Authors
Auld, Allie E
Brouwer, Jack
Samuelsen, G Scott

Publication Date
2012

DOI
10.1016/j.epsr.2011.08.012

Copyright Information
This work is made available under the terms of a Creative Commons Attribution License, availalbe at https://creativecommons.org/licenses/by/4.0/

Peer reviewed

eScholarship.org Powered by the California Digital Library
University of California

Electric Power Systems Research 82 (2012) 44–53

Contents lists available at SciVerse ScienceDirect

Electric Power Systems Research

journal homepage: www.elsevier.com/locate/epsr

Analysis and visualization method for understanding the voltage effect of distributed energy resources on the electric power system

Allie E. Auld, Jack Brouwer*, G. Scott Samuelsen

Advanced Power and Energy Program University of California, Irvine, CA 92697-3550, USA

ARTICLE INFO

Article history:
Received 18 March 2011
Received in revised form 12 August 2011
Accepted 12 August 2011
Available online 24 September 2011

Keywords:
Control strategies
Distributed energy resource (DER)
Distribution system
Dynamic modeling
Inverter
Voltage regulation

ABSTRACT

While adding distributed energy resources (DER) to a distribution circuit will affect numerous aspects of operation, bus voltage is a critical aspect that must be maintained within acceptable limits. It is therefore critical to: (1) quantify how DER installation will affect the voltage, (2) visualize the voltage change, and (3) predict the voltage change of the alternatives within the DER operational space. These three goals are achieved through the development of a simple voltage change potential (VCP) visualization method that can be determined using the basic characteristics of an inverter-based DER installation. The VCP results compare favorably with equivalent complete non-linear Matlab/Simulink™ models of DER implementation in distribution circuits at a fraction of the computational time. Calculation of VCP also enables a new control method that uses circuit information and simple equations to provide situation-dependent and optimal voltage regulation.

© 2011 Elsevier B.V. All rights reserved.

1. Introduction

Distribution systems are built to provide service locations with a voltage that is within a specified range by making assumptions on the direction, magnitude, and time-based characteristics of the real and reactive power load flow. DER can disrupt this process by (1) changing the load flow assumptions and directly creating over- or under-voltages, or (2) conflicting with the control of the utility voltage regulation equipment, such as capacitor banks and step voltage regulators. In the absence of other utility equipment, the first category could be addressed by allowing the DER to make local assumptions about power flow and counter adverse behavior, as shown in the analytical analysis of system voltage perturbations due to DG from [1] or the simulation-based simple circuit analysis in [2]. The added difficulty of the second category – potential fighting between DER and infrastructure – however, creates a complex challenge that limits the integration of high levels of DER in current distribution infrastructure. A report by GE CRD for NREL in 2003 investigated this problem by conducting a comprehensive study on generic distribution feeders to gain insight into the difficulties of integrating distributed generation (DG) into a distribution system [2]. There are a variety of over- and under-voltages in almost all of the cases and this work concludes that voltage regulation cannot be achieved without communications and control in distribution circuits [2]. While the GE/NREL work utilizes a worst-case approach of combining highest generation with lightest load, a stochastic load and generation model from Widen et al. indicates that voltage challenges are infrequent for high penetration residential PV installations under realistic operating scenarios [3]. Conti and Greco [4] examine this problem by assuming a centralized control for a distribution system with high penetrations of synchronous DG. The controller performs a dynamic load flow of the distribution system by using set system parameters as well as real-time utility operating data and DG information. Conti et al. also proposes a local control method in [5] that attempts to eliminate overvoltage problems in photo-voltaic (PV) installations by curtailing the real power if the local voltage exceeds a set limit.

Even if all customer loads are maintained within the allowable voltage limits, the integration of DER into the system can affect the voltage regulating equipment itself. DER could increase the number of times the capacitor bank must switch on and off, which would result in additional mechanical wear on the switch [6]. And Brady et al. describe a scenario where the increased system voltage would reduce the on time of capacitor banks and therefore increase the total import of reactive power from the rest of the electric power system [7].

2. Background

A distributed energy resource (DER) can provide power generation, energy storage, or energy conversion that is typically located near to the site of its use. The most common small generators and storage elements share an additional attribute – they are all inherently DC electricity-based resources. Fuel cells and solar

* Corresponding author. Tel.: +1 949 824 1999; fax: +1 949 824 7423.
E-mail address: jb@nfcrc.uci.edu (J. Brouwer).

0378-7796/$ – see front matter © 2011 Elsevier B.V. All rights reserved.
doi:10.1016/j.epsr.2011.08.012

photovoltaic generators create DC electricity directly, and micro-turbine generators (MTG) have a variable high frequency generator that rectifies to a DC bus. Electric energy storage elements, such as ultracapacitors and batteries are DC sources as well. Thus, while all of these DER have unique behavior and dynamics, they fundamentally connect to the rest of the electric power system in the same way – through a DC/AC inverter. In order to understand how such an inverter-based DER will affect the electric power system, each distribution element must be characterized and combined into a fully integrated feeder system model.

2.1. DER

The distributed generators considered herein include fuel cells (FC), micro-turbine generators, and solar PV. Wind turbines are not included as they are assumed to be interconnected at the transmission level. Fuel cells electrochemically react fuel and oxidant to produce electricity and heat. There are many types of fuel cells, but one categorization is by temperature – two low temperature fuel cell types, such as polymer electrolyte membrane (PEM), and two high temperature fuel cell types [8]. Some applications for the low temperature fuel cells include vehicles and back-up power/combined heat and power (CHP) applications [8]. High temperature fuel cells are well-suited to large, stationary, continuous power applications with CHP [9].

MTG are considered a more mature technology than fuel cells and solar PV because gas turbine technology has been used commercially for both stationary power and propulsion applications for decades. MTG are smaller-scale versions of these common systems that use a slightly different type of compressor in a power output size class that is suited for distributed power and heat generation (e.g., less than 1 MW) [10]. In general, an MTG can change power output, though with a limited dynamic ramp rate, such as 2 kW s^{-1} for the Capstone C60 MTG [11].

Solar PV has very different characteristics compared to an FC or MTG because it is based on an intermittent solar energy resource. While an FC or MTG will have a constant output and potential ability to manipulate output power, the maximum solar PV output is constantly changing in an uncontrollable manner. For a given temperature and solar irradiation level, there is a certain voltage that corresponds to the maximum power output of the cell. Advanced solar power controllers are designed to change the output voltage to achieve this maximum power point, but under certain circumstances it can be reduced to a lower value (if desired). Thus, in the absence of secondary energy storage, solar PV power is not controllable, but it is curtailable through manipulation of the cell voltage [5].

2.2. Power electronics

One characteristic shared by most distributed energy resources is that they rely on an inverter-based connection with the rest of the 3-phase AC electric power system. There are many types of inverters with various grid-connected behavior, although two main categories are multi-pulse inverters and pulse-width modulated (PWM) inverters [12]. In addition, there is interest in integrating a static synchronous compensator (STATCOM) capability into the inverter for use when the real power output is less than the rated inverter capacity. The STATCOM capability would enable the inverter to utilize spare capacity for the production or consumption reactive power as an ancillary service [13,14] or local power factor correction [15]. These additional functions increase the allowable operating modes of the inverter from just the generator-defined real power to the real power plus a reactive power capability that can produce benefits for the electric grid.

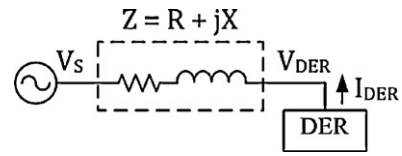

Fig. 1. Two bus circuit schematic for voltage linearization.

2.3. Modeling methodology

Each full nonlinear distribution system is modeled in Matlab/Simulink™ as described in [16]. The model includes a direct three-phase waveform-level simulation as well as a post-processing code to output quantitative parameters such as real/reactive power flows and rms voltage. Both levels of the model have been previously verified against analytical theory, literature data when available, and other commercial load-flow software programs such as PSCAD™ and PowerWorld™.

3. Analysis

3.1. Voltage change potential (VCP) method development

The VCP method is developed by first considering a linearization of a two-bus system. This simplification allows the DER real and reactive power to directly translate into the local voltage change. The voltage drop is calculated with the two-bus system that is presented in Fig. 1. The line impedance is defined as Z, which is the sum of line resistance (R) and reactance (X). The voltage drop ΔV_{DER} is the difference between the magnitude of the DER local voltage, V_{DER}, and the source voltage, V_S (Eq. (1)). The voltage at the DER location is calculated with Ohm's Law (Eq. (2)) using the DER current (I_{DER}), and the resulting voltage drop is defined in Eq. (3). The definition of apparent power, $S = P + jQ = VI^*$, can be used to rewrite I_{DER} as a function of the real and reactive power (P_{DER}, Q_{DER}), and substitute it into the expression for voltage drop (Eq. (3)) to produce Eq. (4). Further manipulation can separate the V_{DER} term into a real and imaginary part as presented in Eq. (5).

$$\Delta V_{DER} = |V_{DER}| - |V_S| \tag{1}$$

$$V_{DER} = V_S + I_{DER}Z \tag{2}$$

$$\Delta V_{DER} = |V_S + I_{DER}Z| - |V_S| \tag{3}$$

$$\Delta V = \left| V_S + \frac{(P_{DER} - jQ_{DER})}{V^*_{DER}}(R + jX) \right| - |V_S| \tag{4}$$

$$\Delta V = \left| V_S + \frac{(P_{DER}R + Q_{DER}X)}{V^*_{DER}} + \frac{j(P_{DER}X - Q_{DER}R)}{V^*_{DER}} \right| - |V_S| \tag{5}$$

In general, generators are considered to be constant P and Q sources, meaning that their real and reactive power output does not depend upon voltage – if the voltage changes, so will the current. Distributed generators will behave in a similar way. However, for the sake of linearization, the DER will instead be interpreted as a constant current source. This is a major, nontrivial assumption that is useful for effect visualization, but will heavily influence the accuracy of the results. The choice of standard DER voltage is another major factor in the subsequent results of the linear approximation. The local voltage is generally assumed to be between 0.95 p.u. and 1.05 p.u., so choosing a standard DER voltage of 1.0 p.u. should minimize the worst possible error. The source voltage is defined as the voltage reference with an angle of 0°, and it is also assumed that the voltage angle between V_S and V_{DER} is negligibly small. The magnitude of the voltage drop equation can then be calculated as

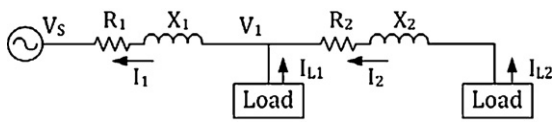

Fig. 2. Three bus circuit schematic for circuit superposition.

presented in Eq. (6).

$$\Delta V = \sqrt{\left(V_S + \frac{(P_{DER}R + Q_{DER}X)}{|V_{DER}|}\right)^2 + \left(\frac{P_{DER}X - Q_{DER}R}{|V_{DER}|}\right)^2} - |V_S| \tag{6}$$

If the voltage drop is assumed to be much smaller than the actual voltage, it follows that the first term dominates over the second term, which can be consequently neglected. Thus the voltage drop can be simplified as a linear combination of real and reactive power, providing the earlier constant V_{DER} assumption. These equations can be rewritten as in Eq. (7), or as in Eq. (8) where two constants K_P and K_Q are defined as in Eqs. (9) and (10).

$$\Delta V = \frac{P_{DER}R + Q_{DER}X}{V_{DER}} \tag{7}$$

$$\Delta V = K_P P_{DER} + K_Q Q_{DER} \tag{8}$$

$$K_P = \frac{R}{V_{DER}} \tag{9}$$

$$K_Q = \frac{X}{V_{DER}} \tag{10}$$

3.2. DER and circuit superposition

The linear relationship between voltage drop and DER real/reactive power could be superimposed over an existing distribution circuit if the distribution circuit was also linear. The distribution circuit can be linearized by making similar assumptions as in the previous section, including that all loads are constant current loads. In reality, most linear loads are a combination of constant impedance and constant power loads. A general rule of thumb is to model loads as 60%/40% constant power/impedance in summer, and 40%/60% constant power/impedance in winter [17]. However, because constant power loads exhibit reduced current with increased voltage, and constant impedance loads exhibit increased current with increased voltage, a 50%/50% constant power/impedance load distribution can be fairly well approximated as a constant current load, which is neutral to voltage change [17].

An arbitrary 3-bus distribution circuit is defined as presented in Fig. 2. The voltage at an arbitrary bus 1 and bus 2 can be determined by the same methodology as in the previous section. I_{P1} and I_{Q1} are the real and reactive current components through the line between bus 1 and bus 2, and I_{P2} and I_{Q2} are the real and reactive current components through the line between bus 2 and bus 1. Assuming that there are two loads, I_{L1} and I_{L2} at bus 1 and bus 2 that have both a real and reactive component, the system of equations can be written as in Eq. (11).

$$\begin{bmatrix} V_1 \\ V_2 \end{bmatrix} = \begin{bmatrix} R_1 & R_1 \\ R_1 & R_1+R_2 \end{bmatrix} \cdot \begin{bmatrix} I_{LP1} \\ I_{LP2} \end{bmatrix} + \begin{bmatrix} X_1 & X_1 \\ X_1 & X_1+X_2 \end{bmatrix} \cdot \begin{bmatrix} I_{LQ1} \\ I_{LQ2} \end{bmatrix} + \begin{bmatrix} V_S \\ V_S \end{bmatrix} \tag{11}$$

Eq. (11) can be rewritten in general vector and matrix notation as in Eq. (12).

$$\vec{V} = \mathbf{R}\vec{I_P} + \mathbf{X}\vec{I_Q} + \vec{V_S} \tag{12}$$

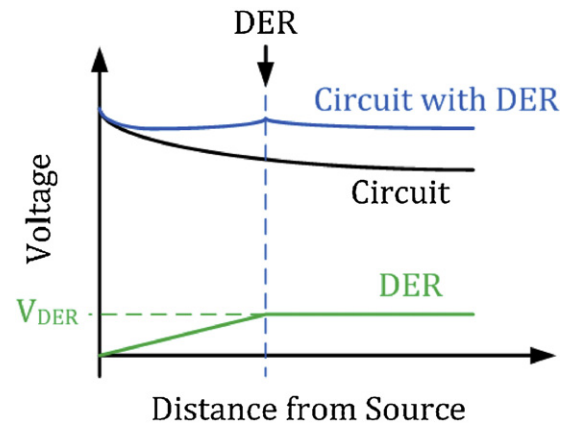

Fig. 3. Superposition of the voltage profiles of a circuit with DER.

By defining $\vec{V} = \vec{V} - \vec{V_S}$, the relationship between load current and voltage can be shown as linear. The change in voltage due solely to DER is written out as in Eq. (13) and the combination of voltage due to circuit load and DER is expressed in Eq. (14). Eq. (14) can be rearranged to equal the sum of the voltage without DER addition plus the change due to DER as in Eq. (15). Thus the entire system can be described as the superposition of the behavior without DER and the pure DER behavior (without other system loads, etc.). This result implies that under certain assumptions, the voltage of a circuit with DER can be described as the voltage of that circuit without DER plus the voltage change that would occur solely due to DER installation (and no other loads). This superposition is illustrated in Fig. 3, where the voltage profile of the circuit with DER is the sum of the profile of the original circuit and that of the DER alone (where the location is marked with an arrow).

$$\overrightarrow{\Delta V} = \mathbf{R} \cdot \vec{I}_{DER,P} + \mathbf{X} \cdot \vec{I}_{DER,Q} \tag{13}$$

$$\vec{V'} = \mathbf{R} \cdot (\vec{I_P} + \vec{I}_{DER,P}) + \mathbf{X} \cdot (\vec{I_Q} + \vec{I}_{DER,Q}) + \vec{V_S} \tag{14}$$

$$\vec{V'} = \mathbf{R} \cdot \vec{I_P} + \mathbf{X} \cdot \vec{I_Q} + \vec{V_S} + \mathbf{R} \cdot \vec{I}_{DER,P} + \mathbf{X} \cdot \vec{I}_{DER,Q} = \vec{V} + \overrightarrow{\Delta V} \tag{15}$$

3.3. Voltage change potential

Eq. (15) infers that the ΔV quantity for the DER alone is also the change in the system due to DER. Thus, we define this term as the voltage change potential (VCP) because it represents the capability of the DER to change a given voltage and is the linear combination of real and reactive power weighted by the impedance parameters K_P and K_Q to the nearest stiff voltage source. When the DG produces only real power (no Q) this value is reduced to $\Delta V_{DER} = K_P P_{DER}$, which is represented by a line through the origin with a slope of K_P. Fig. 4 shows this line, along with a shaded space surrounding the line that represents possible ΔV_{DER} that could be reached through the consumption ($Q < 0$) or generation ($Q > 0$) of reactive power. This shaded region represents the space within which the DG can change the voltage. The border between shaded region and background represents the reactive power limits on the DER inverter. The dotted lines in Fig. 4 indicate the extremes of allowable voltage change limits. If the voltage at the DER location is 1.0 p.u. without DER and the allowable limits are 1.05 p.u. to 0.98 p.u. then the ΔV_{max} would allow a voltage increase of 0.05 p.u. Similarly, the lower voltage limit would be $\Delta V_{min} = -0.02$ p.u.

The local voltage will change throughout the day, either due to changes in local and neighboring load, neighbor circuits, or fluctuations in the rest of the utility system. Thus, the ΔV_{max} and ΔV_{min} limits of the described approach are determined at the DER location at one moment, but will change in time. The range of values that the ΔV_{max} and ΔV_{min} limits can include could be instead realized

Table 1
Line impedances for Circuits A and B.

	First half R (Ω)	First half X (Ω)	Second half R (Ω)	Second half X (Ω)
Circuit A	0.5	1.0	0.8	1.4
Circuit B	1.0	2.0	1.6	2.8

Table 2
Voltage-regulating characteristics for Circuits A and B.

	Capacitor bank rating (kVAR)	Capacitor location (bus #)	LDC setting (Ω)	Nominal voltage (p.u.)
Circuit A	–	–	–	1.05
Circuit B	1200	4, 8, 12, 16	$0.6+j1.1$	1.02

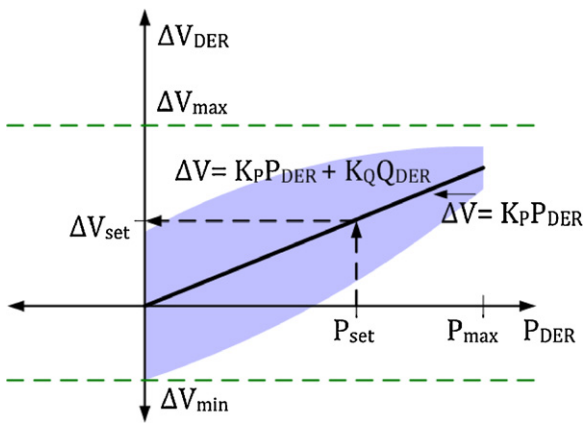

Fig. 4. Conceptual visualization of DER VCP.

as a shaded region that recognizes the variability of these limits. Fig. 5 presents a series of different DER behavior overlayed on these ΔV_{max} and ΔV_{min} regions. This image fundamentally divides DER installations into three categories: completely within, intersecting, and extending beyond this limiting region. DER installations with a VCP that is well under the lowest normal maximum can be relatively insensitive to voltage regulation. This region is termed the "external control" region, because the system may find it valuable to utilize voltage regulation-type assets of the DER – but it would be an external signal. A DER that enters the maximum region can be installed, but must be capable of regulating output to always remain within the region of safe and acceptable operation. And DER installations with a VCP that extends above this region are, in general, not advisable for the particular combination of loading, location, circuit configuration, and DER capacity. There are exceptions, such as a PV array with energy storage that could then be curtailed to remain within safer limits and meet voltage constraints. In addition, an intermittent resource such as PV will have a time-varying power output P_{max} as is described in Section 5.

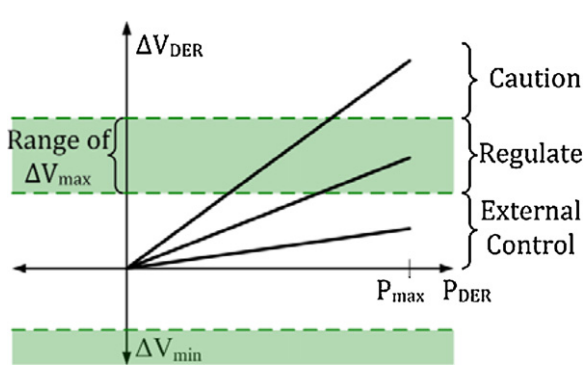

Fig. 5. Conceptual visualization of time-based variation in DER VCP.

4. Comparison of VCP to model simulation

The VCP concept, which uses linearization to quickly determine whether a particular DER installation is advisable, can illustrate the effects of a generator on the rest of the system. Yet the VCP is based on several major assumptions and to determine the relative accuracy of the method, the results predicted from the VCP method are compared with those of a full non-linear model. Two circuits are defined for the sake of comparison: Circuits A and B. Circuit A is 4 miles in length with a constant input substation voltage and Circuit B is 8 miles in length with a substation voltage that changes with load according to a load drop compensation (LDC) transformer. Circuit B also has four 1200 kVAR capacitor banks that are evenly spaced in the circuit. Circuits A and B are defined as for Case 1.1 and Case 2.2 in [2] and as Circuits A and B in [16]. The modeling methodology can be extended to unbalanced, non-uniform load conditions, but because of the generic nature of the two circuit models the loading is assumed to be balanced and uniform. The main characteristics are presented in Table 1 for circuit impedance and Table 2 for capacitor characteristics and transformer behavior.

For each circuit, the VCP linearization is first predicted from the circuit information and then compared to the full non-linear simulation results. The appropriateness of the linearization can therefore be evaluated for a wide variety of DG scenarios. The cases examined include DG lumped at the beginning (bus 1), middle (bus 10), and end (bus 20) of each circuit at different penetration levels (0, 10%, 20%, 30%, 50%, and 100%). The penetration is calculated as the percentage of the circuit base power, which is defined as 7 MVA for both circuits. The constant power load is assumed to be balanced and uniformly distributed between the 20 load buses and spans two values: light load of 2.1 MW at 0.95 pf and heavy load of 7 MW at 0.85 pf. The allowable voltage range is 1.05–0.98 p.u., as is defined in [2]. This allows for the line voltage to drop between the primary and the service entrance and remain above 0.95 p.u.

4.1. Circuit A

For Circuit A, the only impedance parameter between the bus location and voltage source is the line impedance. The substantial differences in magnitude of K_P and K_Q parameters (Table 3) at each of the three locations indicate the three previously described groups: minimal, moderate, and extreme voltage effect.

As there is very minimal impedance between the stiff 1.05 p.u. voltage source and DG location at bus 1, the K_P and K_Q parameters are both quite low. The VCP method predicts that voltage on the

Table 3
K_P and K_Q values for DG locations in Circuit A.

	K_P	K_Q
Bus 1	0.00225	0.0045
Bus 10	0.025	0.045
Bus 20	0.0585	0.108

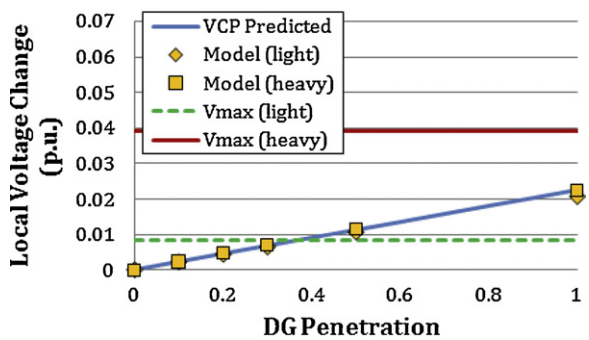

Fig. 6. VCP for DG at the middle of Circuit A.

rest of the circuit will be fairly insensitive to DG deployment. Full simulations of this case were consistent with this prediction and the only voltage problem that occurred for this case was a very slight overvoltage at bus 1 for the case with 100% DG penetration and light load. This occurs because the source voltage is already at the upper limit of acceptable voltage, which gives the DER bus a maximum voltage change of only 0.0011 p.u. for the light load case. The linear model is able to predict the change quite closely for this case, although the change in voltage is on the order of the precision of the model itself at lower penetrations. The error on the higher DG penetration cases has a maximum of 11%.

The higher K_P and K_Q values for bus 10 imply the generator will cause a greater voltage change than at bus 1. Accordingly, the model shows that this case has an overvoltage during light load for penetrations of 50% and 100%. This overvoltage problem is illustrated in Fig. 6 with lines that represent the maximum voltage change at heavy and light load. The V_{max} at light-load line intersects the predicted voltage change line around a DG penetration of 40%, which implies that this is overvoltage threshold. There are no model data at this location, but the 30% DG case is considered acceptable while the 50% case is not. The heavy-load line does not intersect the predicted VCP line, which is consistent with the lack of voltage problems predicted by the full non-linear model at heavy load. The analytical VCP predictions show reasonable agreement with the non-linear results here with the maximum error being 8%, but in a conservative direction – the VCP predicts a worse voltage increase.

K_P and K_Q are very high for the end location, indicating that high penetrations of DG may not be advisable due to voltage concerns. The VCP model predicts severe overvoltage problems for 30%, 50%, and 100% DG penetration cases during light load. Overlaying the light and heavy load V_{max} lines in Fig. 7 indicates that this light load penetration limit may be close to 20%. The model/VCP prediction agreement is reasonable at low penetrations, but is relatively poor for the 100% DG penetration cases – with errors as high as 16% for

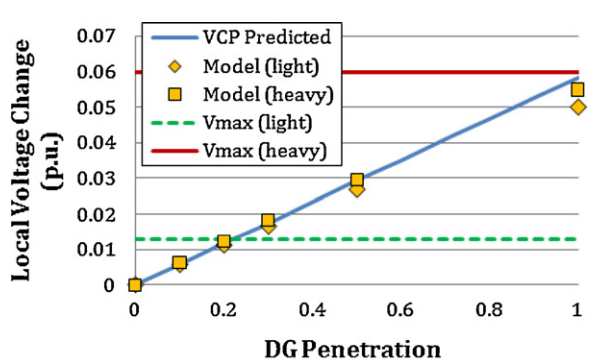

Fig. 7. VCP for DG at the end of Circuit A.

Table 4
K_P and K_Q values for locations in Circuit B.

	K_P	K_Q
Bus 1	−0.0225	−0.0405
Bus 10	0.0180	0.0405
Bus 20	0.0900	0.167

the light load case. This is probably due to the overvoltage itself because the DG bus voltage is at 1.09 p.u., which is quite far from the approximate 1.0 p.u. used in the VCP linearization. The VCP line never intersects V_{max} for the heavy load case, but comes extremely close. Thus only on a rare occasion could the DG produce full rated power output and not cause an overvoltage on the system (in the absence of additional/alternative voltage control for the DG and/or circuit).

4.2. Circuit B

Circuit B is longer and has a more complex infrastructure than Circuit A. The additional length increases the line impedances, which is compensated for by LDC at the substation and capacitors along the line. As the capacitors are fixed, their effect will be accounted for as an uncontrollable negative load and not explicitly included. The LDC, however, uses power flow to change the bus 0 voltage and is therefore of direct importance to the circuit voltage regulation. The LDC affects voltage by compensating for voltage drop, which is approximated by Eq. (16).

$$V_0 = V_{set} - I_{line}(R_{LDC} + jX_{LDC}) \tag{16}$$

The previous sign convention of a positive I_{line} meaning current flowing towards the substation is maintained. Using the earlier line loss decomposition and approximation, the V_0 can be split into a part set by the other circuit parameters and a part determined by the DER effect as presented in Eq. (17).

$$V_0 = \left(V_{set} - \frac{P_{load}R_{LDC} + Q_{load}X_{LDC}}{V_0}\right) - \frac{P_{DG}R_{LDC} + Q_{DG}X_{LDC}}{V_0} \tag{17}$$

Eq. (17) shows that the DG-affected change in voltage at the beginning of the circuit can actually be characterized by a *negative* impedance–power relationship. Each impedance segment of the line, from stiff source to location of interest, must be summed together for the total K_P and K_Q, so these LDC settings must be subtracted from the standard line impedance values. This is fundamentally how the LDC works – it negates the effects of line impedance. The resulting K_P and K_Q values for Circuit B are presented in Table 4.

The case of DG at bus 1 is extremely interesting and important because the K_P and K_Q values are negative. This implies that any attempt to regulate voltage will have a contrary effect on the system. Increasing real power will *decrease* local voltage and producing reactive power will *decrease* the local voltage. This case illustrates why understanding the circuit infrastructure is critical to proper voltage regulation; an appropriate control response in one of the Circuit A cases would have the opposite effect in this Circuit B case. Instead of overvoltage problems, this case exhibits an undervoltage problem for the 7 MW case. The non-linear model predicts a voltage of 0.979, where 0.98 is the limit. The source bus has a larger undervoltage (0.971 p.u.), though no loads are defined at this bus.

The generator changes the voltage at other buses as well as its own location. Because the K_P and K_Q values change with impedance, which is basically distance, a single DG actually has a different VCP at every location between the voltage source and the DG itself. Downstream buses all have the same DG VCP as at the DG location, but they can still have different V_{max} and V_{min} limits. To know those limits, the generator must be able to detect remote bus

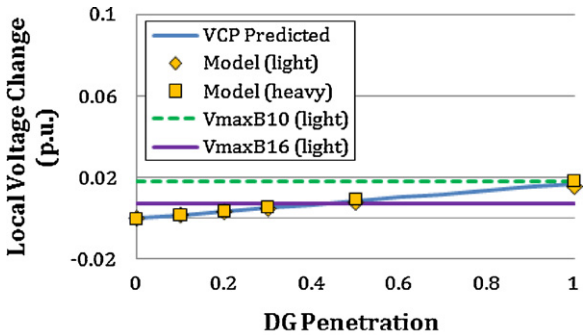

Fig. 8. VCP for DG at the middle of Circuit B.

voltages. Fortunately, the recent surge of activity in smart metering infrastructure could make such remote voltage information readily available in real time.

As the generator location moves sufficiently far from the substation, the line impedance dominates over the LDC parameters and the bus 10 K_P and K_Q parameters are positive. There are still negative K_P and K_Q parameters at bus 1; this is just no longer the local DG bus. As a result, this case creates an overvoltage *and* an undervoltage and both voltage problems occur at locations that are remote from the DER. The undervoltage still occurs for 100% DG at bus 1, but the overvoltage occurs at bus 16/17 for the 50% DG penetration case and at all buses 11 and higher for the 100% DG penetration case. This overvoltage occurs because the capacitor banks at bus 12 and 16 cause a reversed flow of reactive power. Effectively, the allowable voltage rise, ΔV_{max}, of the downstream buses is less than at the DG. These results are presented in Fig. 8, which shows the V_{max} calculated from the local DER bus (bus 10), along with that calculated from the highest voltage at bus 16. For this case, local information at bus 10 would not indicate any overvoltages, when in reality they occur at the 50% and 100% DG penetration levels.

Placing a generator at the end of the line smoothes out some of the complications with installing it at the middle – the massive power reversal washes out the capacitor issue and the highest voltage will be at the DG location. As shown in Fig. 9, the undervoltage problem at bus 1 still exists, but the larger problem is the K_P and K_Q values. The VCP model predicts that for this case, overvoltage problems begin at 10% DG penetration. This is quite a low DG penetration limit, which occurs because of (1) high K_P and K_Q values, and (2) the fixed capacitors – which create a very low ΔV_{max} limit during light load (0.009 p.u). In normal operation, the capacitors raise the voltage at the end of the line by producing reactive power at heavy load. However, when added to DG during the light load condition, the combination raises the line voltage excessively. If the capacitors were removed completely, the line voltage would be allowable when the DG is operable, but unacceptably low when the

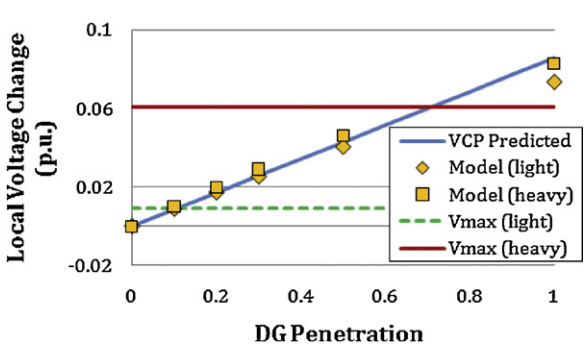

Fig. 9. VCP for DG at the end of Circuit B.

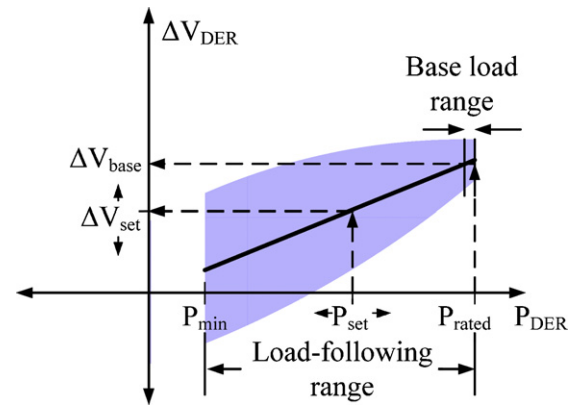

Fig. 10. Illustration of VCP for base-load and load-following DG.

DG is offline. One option is to replace fixed capacitors with switched capacitors, which can be controlled by a variety of strategies.

In addition to overvoltage problems starting at very low DG penetration, the predicted VCP line actually crosses the V_{max} limit for heavy load. Thus a 100% DG penetration would never be able to produce rated real power output without creating a voltage problem, regardless of the circuit load conditions (light to heavy). This does not absolutely mean that this DG should not be installed – reactive power control could reduce this load change, and intermittent DG such as solar PV may be *rated* for a specific power level, but combined with energy storage could be operated to never actually produce a power level anywhere near this value. Still, this DG case falls into the *caution* category because it is, in general, very risky with respect to power quality implications.

Importantly, the results in Figs. 8 and 9 show a very good agreement between the VCP method and use of a full non-linear simulation for analyzing DER installation in the more complex Circuit B. The maximum error between these methods (of 16%) occurs for the light load, 100% DER penetration at the end of Circuit B case.

4.3. Circuit summary

A comparison of DG effects using the VCP method and the full non-linear model has yielded several results:

(1) The VCP analytical expression is capable of capturing the behavior of the full non-linear system to within 16% (worst case) accuracy for a variety of circuits, DER location, and rated capacity.
(2) The K_P and K_Q constants may be positive or negative, thus a generic feedback control developed independent of the value of K_P and K_Q will not be universal.
(3) Because the V_{max}/V_{min} constraints vary, the limiting condition may occur remotely from the DER.
(4) The magnitudes of the K_P and K_Q constants used in the VCP method define the options available for how the DER may interact with the distribution system.

5. Accounting for DER behavior

A general advantage to the VCP-based investigation of DER implementation is that it does not explicitly depend upon the DER type, but can accommodate the main features of the specific installation. For example, a base load fuel cell that can only produce the rated real power output has a VCP that is very narrow and centered at that rated power output (Fig. 10). There may or may not be a shaded region to represent inverter reactive power capability as appropriate to the specific system. This presentation of the VCP

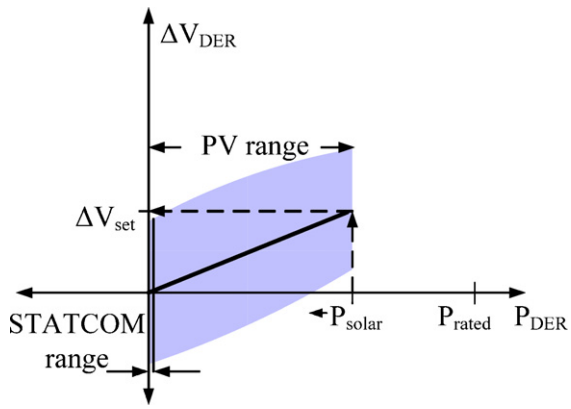

Fig. 11. Illustration of VCP of a solar PV generator and STATCOM operation.

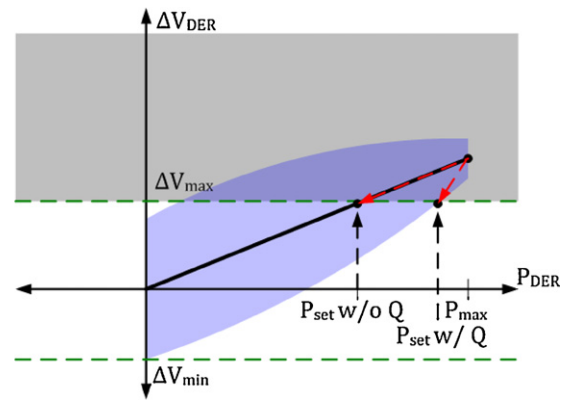

Fig. 13. Control goal for a DG with and without reactive power capability.

method results visually confirms the knowledge that this system is inflexible in its output characteristics. A load-following fuel cell and microturbine generator, however, are each generally capable of reducing output from rated power to a minimum power setpoint. Thus the corresponding VCP ranges from P_{rated} to P_{min} as presented by the larger operating space in Fig. 10.

Solar PV, on the other hand has an output that is always somewhat variable – as P_{solar} (actual) will only rarely coincide with the rated power output of the solar array, P_{rated} and may not be available at all. Yet, due to the inherent characteristics of the PV, the real power output can be turned down from the maximum power point, which is illustrated by the range of real PV power values presented in Fig. 11. Thus the VCP for a solar PV installation has a variable maximum power that is intermittent, uncontrolled, and spans the rated capacity down to 0, which will be the maximum P_{solar} at night. When the real power is 0, the inverter is limited to a pure STATCOM ability as presented in Fig. 11. These conditions represent either solar PV at night or an MTG/fuel cell that is not operated.

Electric energy storage can, in general, either sink or source real power, so it has a 4-quadrant VCP that covers negative power as well, with the maximum charging/discharging rates marking the power boundaries. This 4-quadrant VCP is presented in Fig. 12. This does not capture the *energy* element to electric energy storage and the available power in or out is dependent upon the past charging and discharging of the energy storage device.

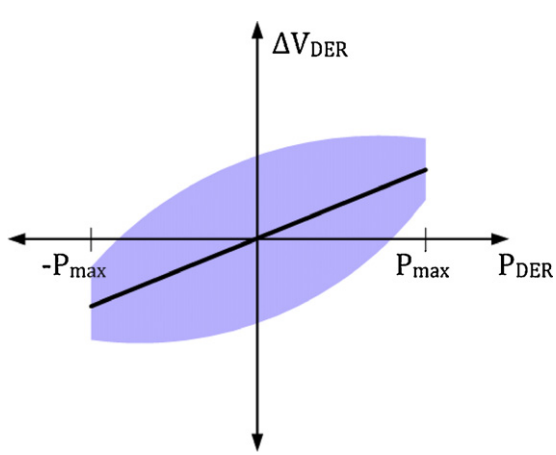

Fig. 12. Illustration of VCP for energy storage.

6. Control strategy

As the VCP visualization has shown fairly good accuracy in predicting the results of DER installation scenarios, it follows that VCP could be used as an estimating strategy for control the DER and inverter itself. The basic premise for VCP-based control is that a combination of external constraints on the system and the time-based system behavior will determine the available operating space of the DER.

If the pre-determined DG setpoint (P_{set}, Q_{set}) falls within this space, the DER will operate at this point. If it falls outside the allowable operating region, this setpoint will be moved to a preferred setpoint located within the space. Herein the real power is prioritized ahead of reactive power, Q – so if the system can maintain P_{set} while changing Q only, it will proceed to do so. If, however, the DER inverter has no reactive power capability, this capability is insufficient, or there are other system constraints that limit the reactive power, then the real power P is curtailed instead. Fig. 13 shows an example of the desired control goal: the setpoint is P_{max} with Q initially set to 0 and the voltage exceeds the permitted system V_{max}. If Q can be generated, the DER may operate anywhere in the oblong shaded region and the new operating point will be where this region intersects the V_{max} limit closest to P_{max}. If there is no reactive power capability, the DER operating point is moved (along the real power line) to where the K_P line intersects the V_{max} limit.

For acceptable DER operation, the real and reactive power must correspond to a VCP that is between the ΔV_{max} and ΔV_{min} boundaries. Using geometry and the linearized equations that define the VCP region, a set of equations can approximate the relation between these voltage boundaries with the controllable parameters P and Q. As maintaining desired real power is prioritized over reactive, the equations are defined such that real power will not be affected unless the reactive power is at its limit. The limits on Q are presented in Eq. (18) and the limits on P are presented in Eq. (19).

$$\frac{\Delta V_{min} - K_P P_{DER}}{K_Q} \le \tilde{Q}_{set} \le \frac{\Delta V_{max} - K_P P_{DER}}{K_Q} \tag{18}$$

$$\frac{\Delta V_{min} - |K_Q Q_{limit}|}{K_P} \le \tilde{P}_{set} \le \frac{\Delta V_{max} + |K_Q Q_{limit}|}{K_P} \tag{19}$$

P_{DER} and Q_{DER} are the actual real and reactive power output of the DER. $\tilde{P}_{set}$ and $\tilde{Q}_{set}$ are the externally defined *desired* inputs into the system. These may either be user-defined setpoints or external inputs, such as a signal to produce/consume reactive power. The accent (tilde) infers that these expressions are linearizations. Q_{limit} is the available reactive power capacity, which is assumed to be symmetric leading and lagging, but the equations can be modified to accommodate non-symmetric values or negative K_P and

Table 5
Summary of DER characteristics for VCP upper and lower bounds.

	Lower bound	Upper bound
Base-load fuel cell	P_{rated}	P_{rated}
Load-following fuel cell MTG	P_{min}	P_{max}
Solar PV	0	P_{solar}
Offline	0	0
Battery	$-P_{max}$	P_{max}

K_Q values. The real power is constrained by the Q limits because it is assumed that the reactive power capacity will accommodate voltage concerns when possible.

Eqs. (18) and (19) define boundaries for the DER in theory, but the ΔV_{max} parameter cannot be directly measured. In a simulation, this value can be calculated by running the identical simulation without DER and recording the nominal voltage at a bus. In a real circuit, the loads and external conditions will be constantly changing and there is no case without DER for comparison. This value can be approximated however, again by using the VCP method to take a local measurement and back calculate what the nominal voltage, V_{nom} (voltage without DG), would be as shown in Eq. (20).

$$\tilde{V}_{nom} = V_{obs} - (K_P P_{DER} + K_Q Q_{DER}) \tag{20}$$

The approximate ΔV_{max} must be calculated from the measured parameter, V_{nom}. V_{nom} is assumed to be a quasi-constant because it is based on the aggregate loads of the distribution circuit. The time-averaged maximum voltage change can be calculated by subtracting V_{nom} from the maximum allowable voltage, V_{max}, as in Eq. (21).

$$\overline{\Delta \tilde{V}_{max}} = V_{max} - \overline{\tilde{V}_{nom}} \tag{21}$$

The estimated nominal voltage is equal to the measured voltage minus the calculated change in voltage due to the DG installation. The approximate reactive power maximum can be combined with Eq. (21) to create Eq. (22), which is a combination of known constants (K_P, K_Q, V_{max}), and known/measureable quantities: V_{obs}, Q_{DER}. A similar expression can be derived for real power, although it must account for the system reactive power limits.

$$\tilde{Q}_{set} \leq \frac{V_{max} - V_{obs} + (K_Q Q_{DER})}{K_Q} \tag{22}$$

In addition to satisfying voltage extremes of the system, the DER characterization must be taken into account. The bounds on real power are defined herein based upon the DER type in accordance with the VCP plots from Section 5. These representative lower and upper boundaries are summarized in Table 5. The reactive power bounds are heavily inverter-dependent and are therefore not considered to be directly affected by the DER type.

6.1. Demonstration of local DER VCP control

The first control strategy relies on the DER local K_P and K_Q values and defines an operating space based on these parameters and local voltage information. Here it is assumed that the desired P and Q are constant values, though they could also be external or user-defined inputs. If the VCP predicts that an undesirable operating state would occur for this operation, the DG P and/or Q values will be changed according to Eqs. (18) and (19) to reach an allowable state. Here the real power is set to 100% of rated capacity and the reactive power is set to 0, though the inverter is sized to allow a power factor of 0.9 leading or lagging at rated power. After the voltage-based constraints on the system are calculated, the DG physical limitations, which includes generator output range and reactive power limits, are applied as well. The resulting P and Q reference signals are then provided as inputs to the DG.

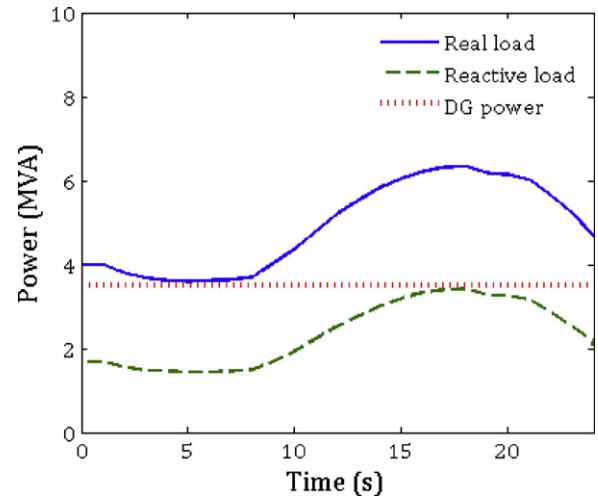

Fig. 14. Load demand and DG power for Circuits A and B.

The utility of the local VCP control is exhibited by comparing the simulation results for (1) baseline control (all real power) and (2) local VCP control applied to a Circuit A undergoing a 24 s power transient. The transient is chosen as a scaled representation of the quasi-steady 24-h power fluctuation for California and presented in Fig. 14. In both baseline and local VCP control cases, the full nonlinear circuit model is used to simulate the feeder with a constant 3.5 MW (50%) generator at the end location. The simulation predicts the resulting voltage for all circuit locations and the resulting minimum and maximum extremes are presented in Fig. 15.

Circuit A exhibits an overvoltage between 1 and 9 s for the baseline control case, but the overvoltage is eliminated with local VCP control. Both control strategies have a real power import that is 3.5 MW below the original demand and the reactive power import is not modified in the baseline case and only increased slightly during the 1–9 s interval. For this case, the local VCP control acts to load level the reactive power demand and increase the minimum. Though as indicated by the drop in load corresponding to an overvoltage, light load conditions will generally be more challenging for overvoltage problems.

6.2. Demonstration of circuit VCP control

Local VCP control only addresses the DER location, but the approach for the VCP control strategy is well-suited to extension

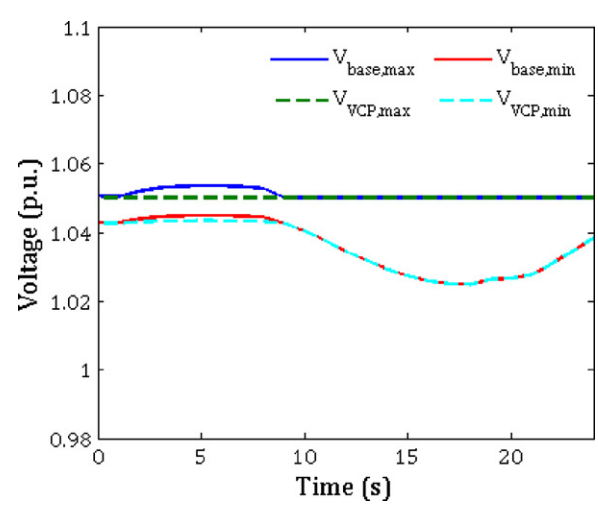

Fig. 15. Voltage for Circuit A with baseline and local VCP control.

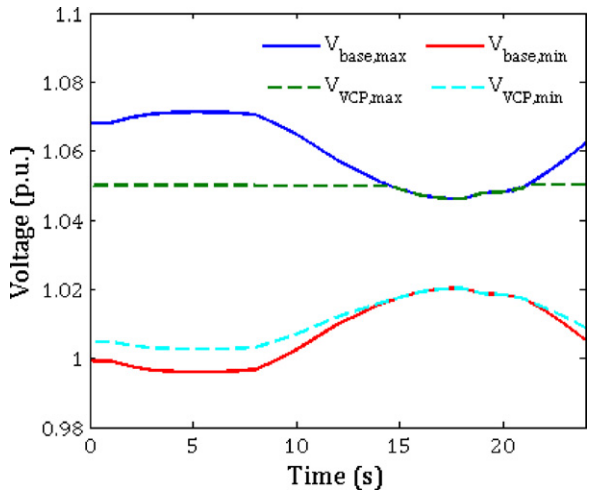

Fig. 16. Voltage for Circuit B with baseline and circuit VCP control.

for other locations. Each bus that has a voltage measurement also has a K_P and K_Q value, which can create a unique VCP plot for that location. The K_P/K_Q values for locations between the DER and source are calculated from the sum of impedance between that location and the source, while locations further downstream from the DER have the same values as those at the DER location. The most constraining P and Q boundaries across all locations are then used to affect the local P and Q setpoint. The resulting circuit VCP control combines the more complete circuit information to refine the desired operating space compared to local VCP control.

Circuit B has voltage regulating equipment installed remotely from the substation and DER and can demonstrate the ability of circuit VCP to detect voltage concerns and provide corrective action. A 3.5 MW capacity generator is installed at the end of Circuit B and causes overvoltages with baseline control. When circuit VCP control is applied to Circuit B, the overvoltages are completely eliminated, as presented in Fig. 16. Circuit VCP also increases the minimum voltage and causes an overall flatter profile throughout the load transient. The real power is approximately equal for both cases and the reactive power swing is again reduced. The real and reactive power flows for both baseline control and circuit VCP control cases are presented in Fig. 17.

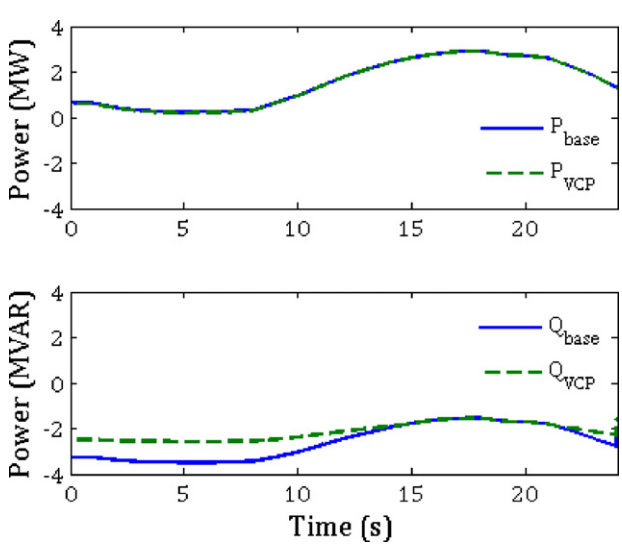

Fig. 17. Real and reactive power importation for Circuit B with baseline and circuit VCP control.

7. Conclusions

A simple method for analyzing and visualizing the effect of DER implementation on an existing electric distribution circuit is proposed and verified using a full non-linear model of various distribution circuits. The method, dubbed the voltage change potential (VCP) method, combined with measured circuit voltage data, can both provide insight into categories of DER installation and illustrate the available operational space for smart inverters. While the VCP linearization relies on several major assumptions, the agreement with a full non-linear model is within 16% for all cases analyzed. Two control methods are developed by using the VCP determined available design space to influence the inverter setpoint. Inherent feedback in the voltage measurement ensures that the inaccuracies in the VCP prediction will be resolved in the physical operation. Both control methods rely on calculating VCP, but the local control only calculates this value locally, while the circuit control relies upon voltage feedback from elsewhere on the circuit. The VCP-based control methods are demonstrated on two full non-linear feeder models and are found to effectively eliminate voltage problems that could occur as a result of DER.

Acknowledgements

The current work was partially supported by the Engineer Research and Development Center of the U.S. Army Corps of Engineers under Contract #: W9132T-08-C-0003 with the Construction Engineering Research Laboratory. The authors thank Frank Holcomb and Nick Josefik for their technical and administrative support.

References

[1] S. Conti, S. Raiti, G. Tina, Small-scale embedded generation effect on voltage profile: an analytical method, IEEE Proceedings: Generation, Transmission and Distribution 150 (1) (2003) 78–86.
[2] GE CRD, DG Power Quality, Protection and Reliability Case Studies Report, submitted to NREL by GE CRD, Contract No NAD-1-30605-01, Program: Reliable, Low Cost Distributed Generator/Utility System Interconnect, August 2003.
[3] J. Widén, et al., Impacts of distributed photovoltaics on network voltages: stochastic simulations of three Swedish low-voltage distribution grids, Electric Power Systems Research 80 (12) (2010) 1562–1571.
[4] S. Conti, A.M. Greco, Innovative voltage regulation method for distribution networks with distributed generation, in: CIRED 19th International Conference on Electricity Distribution, 21–24 May, 2007.
[5] S. Conti, et al., Local voltage regulation in LV distribution networks with PV distributed generation, in: SPEEDAM 2006, International Symposium on Power Electronics, Electrical Drives, Automation and Motion, 2006.
[6] R.A. Walling, et al., Summary of distributed resources impact of power delivery systems, IEEE Transactions on Power Delivery 23 (3) (2008) 1636–1644.
[7] P. Brady, C. Dai, Y. Baghzouz, Need to revise switched capacitor controls on feeders with distributed generation, in: Transmission and Distribution Conference and Exposition, 2003 IEEE PES, 2003.
[8] J. Larminie, A. Dicks, Fuel Cell Systems Explained, second ed., John Wiley & Sons Ltd., 2005.
[9] M.C. Williams, et al., Solid oxide fuel cell technology development in the U.S, Solid State Ionics 177 (2006) 2039–2044.
[10] C.D. Bolszo, Investigation of atomization, mixing and pollutant emissions for a microturbine engine, The UCI Undergraduate Research Journal (2005) 13–22.
[11] F. Mueller, et al., Synergistic integration of a gas turbine and solid oxide fuel cell for improved transient capability, Journal of Power Sources 176 (2008) 229–239.
[12] F.R. Bergseth, S.S. Venkata, Introduction to Electric Energy Devices, Prentice-Hall, Inc., Englewood Cliffs, NJ, 1987, p. 370.
[13] T. Jin, X. Chen, K.M. Smedley, A new one-cycle controlled FACTS element with the function of STATCOM and active power filter, in: Industrial Electronics Society, 2003. IECON 03. The 29th Annual Conference of the IEEE, 2003.

[14] T. Jin, L. Li, K. Smedley, A universal vector controller for three-phase PFC, APF, STATCOM, and grid-connected inverter, Applied Power Electronics Conference and Exposition 1 (2004) 594–600.
[15] G. Tsengenes, G. Adamidis, Investigation of the behavior of a three phase grid-connected photovoltaic system to control active and reactive power, Electric Power Systems Research 81 (1) (2011) 177–184.
[16] A.E. Auld, et al., Effect of distributed generation on voltage levels in a radial distribution network without communication, in: ASME Fuel Cell 2009, Newport Beach, CA, USA, 2009.
[17] H.L. Willis, Power Distribution Planning Reference Book, second ed., Marcel Dekker, New York, NY, 2004.